IEEE Access
Multidisciplinary | Rapid Review | Open Access Journal

Received January 15, 2018, accepted March 19, 2018, date of publication April 24, 2018, date of current version May 16, 2018.

Digital Object Identifier 10.1109/ACCESS.2018.2827199

End-Fire Surface Wave Antenna With Metasurface Coating

PING WANG[1,2] AND ZHONGXIANG SHEN[1], (Fellow, IEEE)
[1]Shool of Electrical and Electronic Engineering, Nanyang Technological University, Singapore 639798
[2]School of Communications and Information Engineering, Chongqing University of Posts and Telecommunications, Chongqing 400065, China

Corresponding authors: Ping Wang (wp@cqupt.edu.cn) and Zhongxiang Shen (ezxshen@ntu.edu.sg)

ABSTRACT This paper describes a wideband and low-profile end-fire surface wave antenna embedded into a large metallic platform. It consists of a tapered grounded slab fed by a wideband surface wave launcher and coated with a planar gradient metasurface (MS). It is found that by altering the surface reactance of the MS array, the surface wave propagating in the grounded slab can be manipulated to suppress the radiation of TM_1 mode region at a specific high frequency. A simple design procedure of MS array is then developed. In addition, a blind-filled cylinder hole is used to further improve the radiation pattern at certain high frequencies. A prototype of the proposed antenna is finally fabricated and tested. Measured results are in good agreement with simulated ones, and they show that the surface wave antenna has a very wide bandwidth from 3.78 to 18.54 GHz for voltage standing wave ratio < 2.5 and exhibits a low profile of only 5 mm ($0.063\ \lambda_L$, λ_L is the free-space wavelength at the lowest operating frequency). Good radiation pattern and high gain are achieved over a wide frequency band.

INDEX TERMS End-fire antenna, gradient metasurface, surface wave antenna, wideband antenna.

I. INTRODUCTION

Wideband end-fire antenna has received growing attention due to its wide applications in aircraft, missile, and unmanned aerial vehicles. It is usually required to be low profile and conformal with curved surfaces of the mounting platform so as to decrease the aerodynamic drag. A lot of efforts have been made to design wideband and low-profile end-fire antennas based on these applications [1]–[5]. In [1], a balanced antipodal Vivaldi antenna was proposed as an array element to be mounted on a large conducting cylindrical platform achieving an extremely broad bandwidth. In [2], an H-plane horn antenna based on a coaxial-to-ridged waveguide transition was studied, and its conformal six-element array placed on the surface of a cylindrical platform was demonstrated in [3]. The antenna achieves a low profile of $0.07\ \lambda_L$ (λ_L is the free-space wavelength at the lowest operating frequency) and a broad bandwidth of 6.6 GHz to 18 GHz with a voltage standing wave ratio (VSWR) less than 2.5. Monopole log-periodic antenna array [4] was designed on a large conducting plane. Each element of the antenna is loaded at the top end with different sizes of patches to reduce the height of the monopoles. Many rows of coupled resonators and directors fed by a trapezoidal launcher were also developed to design a low profile end-fire antenna [5], which exhibits a bandwidth of 109% and a profile of $0.044\ \lambda_L$. However, these proposed designs usually cause aerodynamic drags owing to the fact that they cannot be embedded into the mounting platforms. Surface wave antenna is another candidate to meet the requirements of low-profile, wideband, and end-fire radiation pattern. It is known that a grounded dielectric slab can support TM surface wave propagation. However, when the surface impedance is varied or the dielectric slab is tapered, TM surface wave can be transformed into radiated space wave [6]. Many studies were conducted on the tapered surface wave antenna, such as the impact of curvature on the radiated field and impedance match [7], [8], efficiency of the feeding arrangements and edge diffraction [9], and effect of the dielectric parameters on the attenuation constant and phase velocity of every surface wave mode [10]. However, the designed bandwidth is usually less than 3:1 because TM higher-order modes begin to propagate and radiate at higher frequencies [10] which deteriorates the antenna's radiation pattern and limits its single-mode operational bandwidth. Unfortunately, the suppression of higher-order modes in surface-wave antennas has not been reported in the open literature.

On the other hand, two-dimensional (2-D) metasurface (MS) has been widely used in antenna design owing to its extraordinary EM properties, including bandwidth

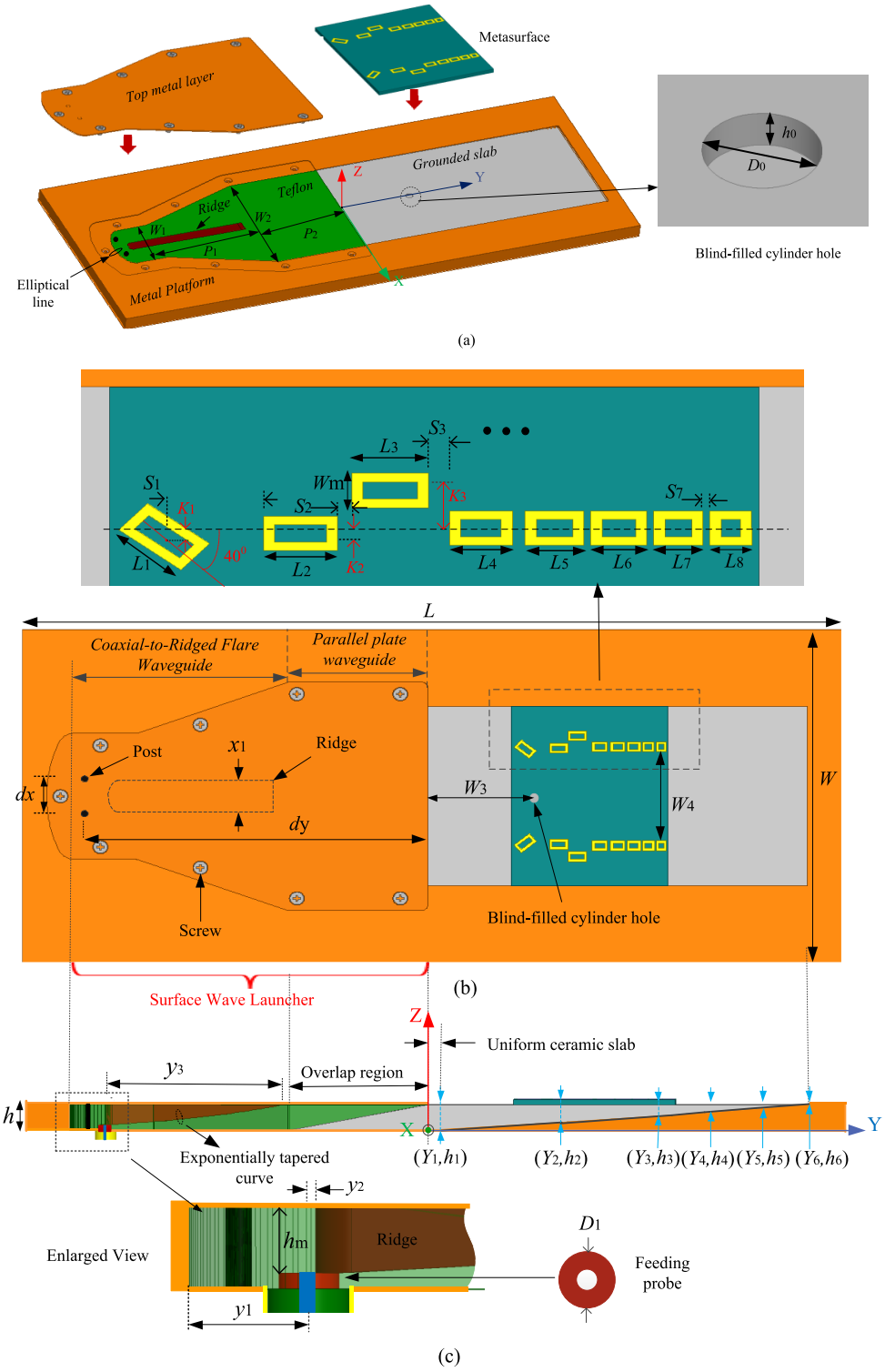

FIGURE 1. Configuration of the proposed low-profile surface-wave antenna. (a) Perspective view. (b) Top view. (c) Side view.

enhancement or size reduction [11], directivity improvement [12], polarization conversion [13], beam refraction [14], filtering functionality [15]–[17], and so on. The filtering property of the MS is similar to that of the frequency selective surface (FSS), in which an incident wave may induce electric and magnetic surface currents on the MS [18]. The surface currents in turn produce the scattered fields on both sides of the MS, which may be explored to improve the radiation pattern of the antenna by changing the shape and periodicity of the MS.

The objective of this paper is to provide a technique of improving the radiation beam in surface-wave antennas by coating it with the MS, while retains its low-profile structure. It will be demonstrated that eight rows of non-uniform rectangular loop with gradually decreasing lengths along the end-fire direction are employed and located at the strongest radiation area of TM_1 mode. The induced electric currents on the MS can change the surface impedance at the air-to-dielectric interface, and in turn control the magnitude and phase of the transmitted field. A blind-filled cylinder hole (BFCH) embedded in the grounded slab is also utilized to further improve the radiation pattern at certain high frequencies. With the proposed techniques, a wideband and low-profile surface-wave antenna is realized. All simulated results are obtained by using ANSYS HFSS. The experimental data of the proposed surface-wave antenna is in good agreement with the simulated results, which validates the effectiveness of the proposed techniques.

II. ANTENNA GEOMETRY

Fig.1 shows the geometry of the overall antenna prototype, including MS coating and BFCH. The antenna consists of three parts: a surface wave launcher, a grounded slab, and gradient MS. The surface wave launcher is a transition between coaxial probe and grounded Teflon slab with a dielectric constant of 2.2. In order to widen the bandwidth of the launcher, a section of ridged waveguide is introduced into the transition [2], [19]. The grounded slab includes two sections: a uniform section (Y_1) and a tapered section (Y_6-Y_1), both inserted into a parallel-plate waveguide of the surface-wave launcher. The bottom layer is ceramic material with a dielectric constant of 25, while the top layer is Teflon. The thickness of the surface-wave launcher is 5 mm, which has the same height as the grounded ceramic slab. A pair of posts is employed to suppress TE_{30} higher-order mode in the flare waveguide. This structure is effective to excite TM surface mode in the uniform ceramic slab. The exponential profile of the tapered ridge can be expressed as

$$z = C_1 \exp(ky + C_2) \tag{1}$$

where $C_1 = h_m/(\exp\left(k(y_2 + y_3)\right) - \exp(ky_2))$, $C_2 = h_1 - C_1\exp(k(y_2+y_3))$. The final antenna is embedded into a large aluminum platform with the same top surface. The size of the platform is about 100 mm (W) × 233 mm (L) × 8.5 mm (h). An SMA connector is used as the feeding source with its inner conductor being inserted into a hollow metallic cylinder that has a height of $h_{01} = h_1 - h_m$ and diameter of D_1, and connected with the starting part of the ridge, and the outer conductor being connected to the bottom surface of the metallic platform.

To improve the radiation beam in higher frequency, we introduce a planar gradient MS array, illustrated in Fig.1 (b). The MS array consists of 16 unit cells arranged in a 2 × 8 array. These non-uniform rectangular loop resonators are placed symmetrically on the strongest field points of TM_1 mode along the x-axis. The length of the loop and gap between two adjacent loops in the ith row are denoted as L_i and S_i (i = 1, 2, 3, 4, 5, 6, 7, 8), respectively. All the loops have the same width of W_m. The MS array is fabricated on a 0.508-mm-thick Taconic TLY substrate with a dielectric constant of 2.2 and loss tangent of 0.0009, and then is placed on the top surface of the ceramic slab directly. In addition to the MS array, a BFCH (with diameter of D_0 and depth of h_0 in Fig.1 (a)) is etched on the ceramics slab along the y-axis, which may help to confine the radiation of TM higher-order mode for achieving a good radiation pattern at certain high frequencies.

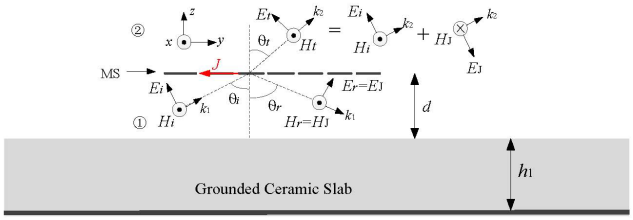

FIGURE 2. Transmission and reflection under oblique incidence of TM wave on the MS.

III. ANTENNA DESIGN AND CONSIDERATIONS

A. THEORETICAL ANALYSIS

For a grounded dielectric slab, the relationship between slab thickness h_1 and surface wave's operating wavelength can be expressed as [20]

$$\frac{h_1}{\lambda} \geq \frac{m}{2\sqrt{\varepsilon_{r1} - 1}}, m = 0, 1, 2 \ldots \tag{2}$$

where ε_{r1} is the dielectric constant of the ceramic slab, λ is operating wavelength in free space. It is well known that only dominant TM_0 mode can be radiated when the thickness of the dielectric slab reaches $\lambda/4\sqrt{\varepsilon_{r1}}$[7], while the main radiating location of the first and second high-order modes TM_1 and TM_2 can be confirmed at the thickness of $3\lambda/4\sqrt{\varepsilon_{r1}}$ and $5\lambda/4\sqrt{\varepsilon_{r1}}$, respectively. Assuming a radiated TM plane wave ($E_x = H_y = H_z = 0$) produced by a slab thickness of $3\lambda/4\sqrt{\varepsilon_{r1}}$ (including TM_0 mode and TM_1 mode) or $5\lambda/4\sqrt{\varepsilon_{r1}}$ (including TM_0 mode, TM_1 mode, and TM_2 mode) incident at an angle θ_i on a 2-D MS at a specific high frequency, as illustrated in Fig.2. The electromagnetic boundary condition on MS can be given as [21]

$$\vec{E}\Big|_{avg}^{y} = Z_{es}\hat{z} \times \left(\vec{H}_2 - \vec{H}_1\right), \tag{3}$$

$$0 = \hat{z} \times \left(\vec{E}_2 - \vec{E}_1\right) \tag{4}$$

where $\vec{E}\Big|_{avg}^{y}$ is the average electric fields on the MS surface, and the electric surface impedance of the MS surface is $Z_{es} = Re\,(Z_{es}) + jIm(Z_{es})$. Owing to the passive MS condition, we obtain (5) and (6), as shown at the bottom of the next page,

where $\phi_1 = k_1 sin\theta_i y - (k_2 sin\theta_t y + \varphi_1)$, $\phi_2 = k_1 sin\theta_i y - \varphi_2$, $te^{j\varphi_1} = H_t/H_i$, $re^{j\varphi_2} = H_r/H_i$, $0 \leq \theta_i, \theta_t \leq \frac{\pi}{2}$, $\theta_r = 0$, $\eta = 377\Omega$, and $0 < t, r < 1$. According to (5), $2n\pi - \frac{\pi}{2} < \phi_{1,2} <$

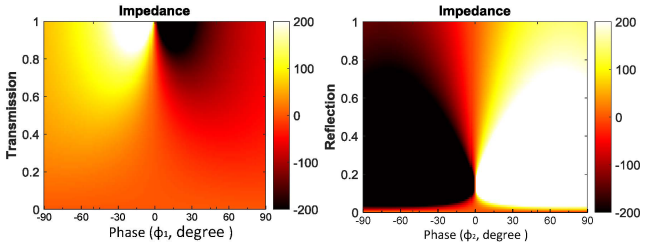

FIGURE 3. Transmission coefficient and reflection coefficient as functions of the surface reactance and the phase.

$2n\pi + \frac{\pi}{2}, n = 0, 1, 2, \ldots$ Fig.3 illustrates the transmission coefficient (t) and reflection coefficient (r) as functions of the surface reactance and the phase, respectively. It is clearly seen that the magnitude and phase of the transmitted and reflected TM wave can be controlled by varying the electric surface reactance of the MS from negative to positive.

B. DESIGN OF THE MS ARRAY

In order to realize such a suitable impedance surface, the E-field distributions on the top surface of the ceramic slab at several frequencies of 5 GHz, 10 GHz, 12 GHz, 14 GHz, 16 GHz, and 18 GHz, are presented in Fig.4. As expected, in addition to TM_0 mode, more than one higher-order modes are excited at different positions for different frequencies above 10 GHz. With the increasing frequency, the positions of TM higher-order modes shift toward the end-fire direction (along the positive y-axis direction).

Based on the above understanding, the design procedures are summarized as follows.

1) Rectangular loop is used as the MS array element owing to its multi-mode resonance and compact cell size. Each loop and the space between adjacent loops produce a series LC resonant circuit so as to provide the needed surface reactance, and control or reduce the transmission of the radiated TM wave. Therefore, the loop size is selected to be about one-wavelength based on the frequency requirement initially.

2) Only TM_1 mode and TM_0 mode is considered here for simplification. The initial distributions of the MS array can be determined according to the strongest E-field region of the excited TM_1 mode, as marked in Fig.4. Moreover, all MS are arranged in a straight line along the y-axis and have a symmetrical configuration along the x-axis owing to the antenna symmetric nature.

3) Location and quantity of the MS array shall be determined. Since a small radiated power of TM_1 mode below 12 GHz is observed in Fig.4, a frequency range from 12 GHz to 18 GHz is chosen. According to (2), the covering region of the TM_1 mode from 12 GHz to 18 GHz is overlapped with that of TM_0 mode from 4 GHz to 6 GHz. In order to decrease the effect of the MS on the radiation of TM_0 mode from 4 GHz to 6 GHz, a small quantity of MS is used in the design. Firstly, the first row and the eighth row of loops, which are corresponding to the frequencies of 12 GHz and 18 GHz, are determined. Secondly, the locations of the loops operating in 14 GHz and 16 GHz are confirmed, and then smooth the length of all loops from 12 GHz to 18 GHz. Ultimately, an optimum gain pattern over the entire band can be achieved by adjusting the length of the loop and the space between adjacent loops using HFSS. It is found that symmetric eight loops are enough to produce a good gain pattern. It is noticed that the distance between adjacent loops in the y-direction is designed as an inhomogeneous structure, which may attribute to the irregular curved ceramic slab.

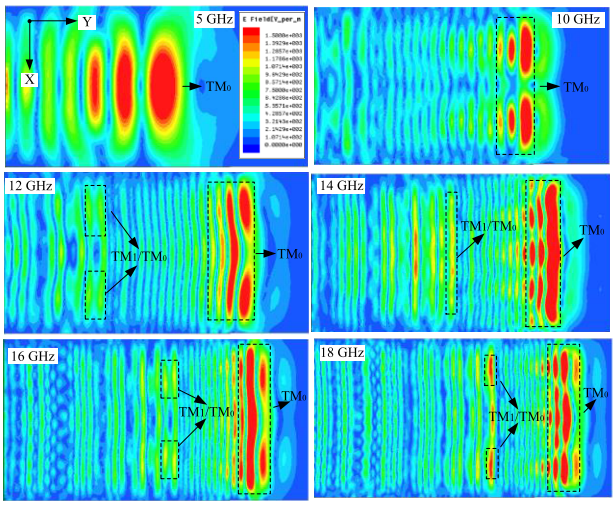

FIGURE 4. Radiated E-field distributions on the top surface of the ceramic slab at several frequencies.

4) Effect of some loops on the end-fire pattern and impedance match at lower frequencies should also be considered so that the locations of these loops need to be redistributed. Radiation pattern shall be determined by the loop dimensions, relative distance between adjacent loops including horizontal and longitudinal distance. It is noticed that the final loop size is slightly larger than one wavelength owing to the oblique incident TM wave.

$$\mathrm{Re}\,(Z_{es}) \geq 0, \quad cos\phi_{1,2} \geq 0, \tag{5}$$

$$\begin{aligned} I_m\,(Z_{es}) &= \frac{-\eta cos\theta_t\,(1+cos\theta_i)\,sin\phi_1 t}{[(1+cos\theta_i)\,cos\phi_1 - t\,(1+cos\theta_t)]^2 + (1+cos\theta_i)^2\,(sin\phi_1)^2} \\ &= \frac{\eta r sin\phi_2 cos\theta_t (1+cos\theta_i)}{[(1+cos\theta_t)\,r]^2 + (cos\theta_t - cos\theta_i)^2 + 2r(1+cos\theta_t)(cos\theta_t - cos\theta_i)cos\phi_2} \end{aligned} \tag{6}$$

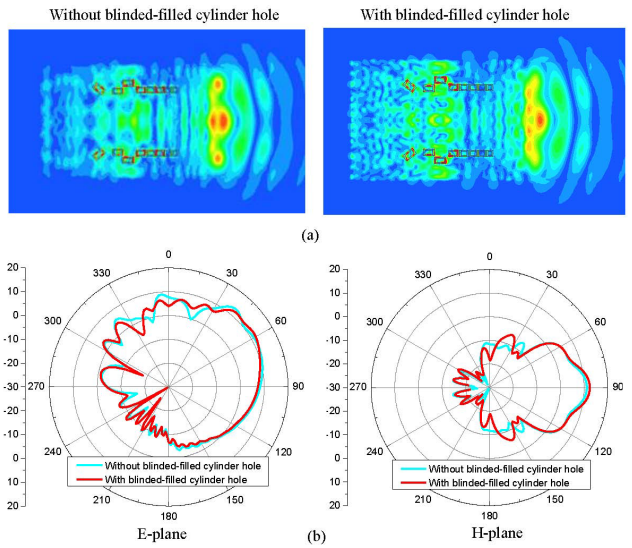

FIGURE 5. Comparison between the surface wave antennas with and without the BFCH at 14 GHz. (a) E-field distributions on the top surface. (b) Radiation pattern in E-plane and H-plane.

C. EFFECT OF THE BFCH

From the above-optimized results, it is found that the side-lobe level (SLL) is still high at 14 GHz. In order to improve the SLL at 14 GHz, a BFCH is introduced as a discontinuity. The mechanism of the discontinuity is similar to that of a waveguide discontinuity, where the loaded region can be seen as inductively loaded element on the top dielectric-free-space interface. If the BFCH is placed at a suitable location $(0, W_3)$ around the strongest radiation region of TM higher-order modes, the open-circuit terminal is transformed into a short circuit or the radiation condition in the loaded region is not satisfied. Therefore, the radiation of higher-order mode at 14 GHz can be controlled by parameter W_3. Fig.5 shows the comparison of the E-field distributions and radiation patterns with and without the BFCH. It is observed that when the BFCH is used, the field distribution of TM higher-order mode region is changed and becomes more uniform compared with that without the BFCH so as to achieve a good E-plane radiation pattern, whereas the H-plane pattern almost keeps no change. It is worth noting that a small diameter D_0 should be utilized for reducing the effect of the BFCH on the radiated field and impedance match at other frequencies.

D. GAIN PATTERN COMPARISON WITH AND WITHOUT MS AND BFCH

All parameters of the proposed surface-wave antenna are carefully tuned and finalized to obtain an acceptable radiation pattern over the entire band, and the optimized parameters are presented in Table 1. Fig.6 shows the simulated radiation patterns comparison with and without the MS and BFCH to exemplify the effectiveness of the proposed method. It is noted that the simulated cross-polarization level is at least 17 dB lower than co-polarization level, especially in the end-fire direction. Therefore, only the co-polarization patterns are presented. In the E-plane, the main beam of the surface-wave antenna without the MS and BFCH is distorted greatly and the maximum radiation beam is deviated from the end-fire direction at a large angle at 12 GHz and 14 GHz owing to the effect of the undesired higher-order mode. As the frequency increases, many high side lobes are produced, i.e., the first SLL is only 3.8 dB less than the main beam at 17 GHz. However, when the MS and BFCH are used, the SLL is decreased greatly and a good main beam is also achieved. In the H-plane, almost stable radiation patterns are obtained at 10 GHz and 17 GHz. However, a large difference is observed at 12 GHz and 14 GHz. It is because the slant angle of the

TABLE 1. Geometric parameters of the proposed surface wave antenna.

Parameter	Value (mm)	Parameter	Value (mm)	Parameter	Value (mm)	Parameter	Value (mm)
L_1	5.8	L_8	3	S_7	0.5	Y_1	3
L_2	5.3	S_1	6.8	W_3	31	Y_2	33
L_3	5.5	S_2	0	W_4	29	Y_3	63
L_4	4.5	S_3	1.5	D_0	2	Y_4	74
L_5	4.2	S_4	0.9	D_1	1.8	Y_5	89.5
L_6	4	S_5	0.5	dx	11.2	Y_6	110
L_7	3.5	S_6	0.5	dy	99.1	h_0	0.5
h_2	3.75	h_3	2.715	h_4	2	h_5	1
h_6	0.2	K_1	0.6	K_2	0.5	K_3	3.5
Wm	3.2	hm	4.07				

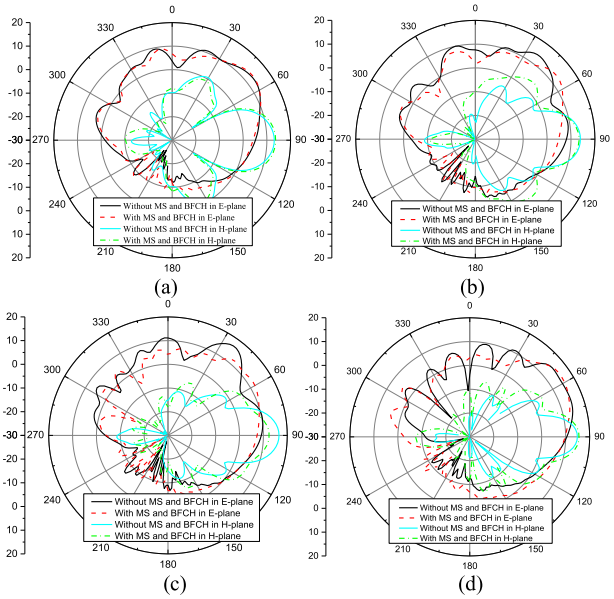

FIGURE 6. Comparison of simulated radiation pattern of the proposed surface wave antenna with and without the MS and BFCH at (a) 10 GHz, (b) 12 GHz, (c) 14 GHz, (d) 17 GHz.

FIGURE 7. Photograph of the proposed surface-wave antenna prototype mounted inside an anechoic chamber.

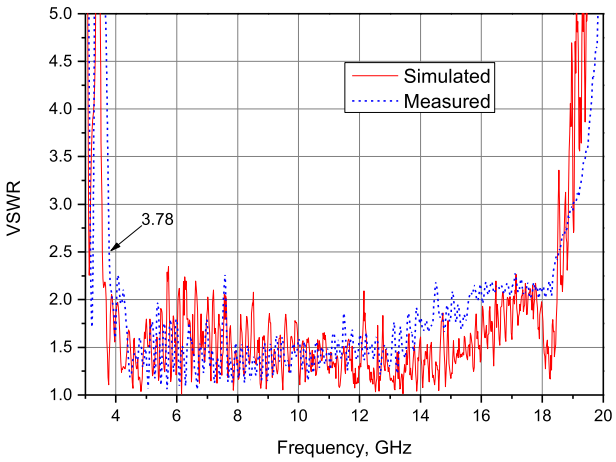

FIGURE 8. Simulated and measured VSWR results of the proposed surface wave antenna.

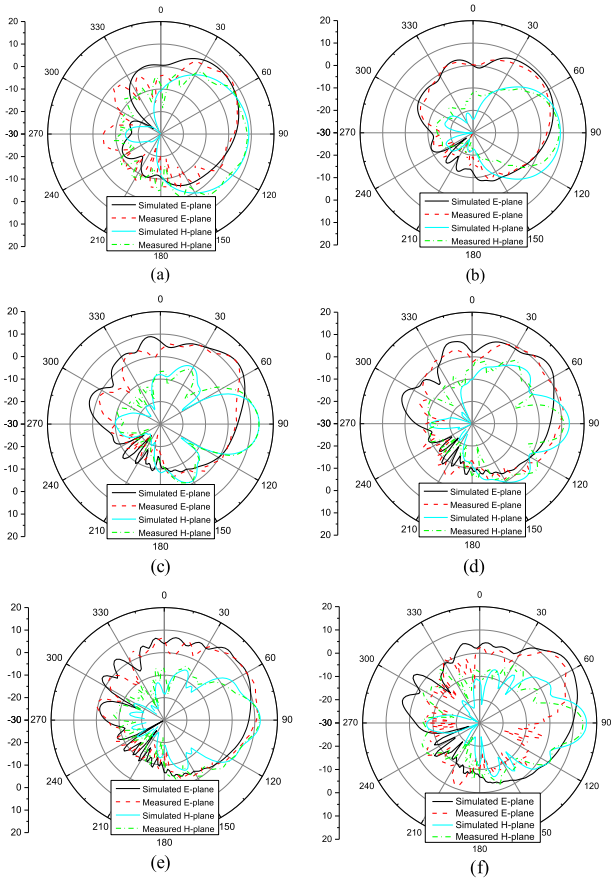

FIGURE 9. Simulated and measured radiation patterns of the proposed antenna at (a) 4 GHz, (b) 7 GHz, (c) 10 GHz, (d) 12 GHz, (e) 14 GHz, (f) 17 GHz.

H-plane without the MS and BFCH is different with that with the MS and BFCH owing to different main beam angles. For example, the slant angle is 52° for 12 GHz and 54° for 14 GHz without the MS and BFCH, whereas the slant angle is 38° for 12 GHz and 30° for 14 GHz with the MS and BFCH. It can be concluded that the proposed method is effective in suppressing TM higher-order mode produced in a thick grounded slab.

IV. SIMULATED AND MEASURED RESULTS

A prototype of the designed surface-wave antenna is fabricated and tested, as shown in Fig.7. Some screws are used to fix the top conducting layer on the metallic platform, which have no effect on the antenna's radiation performance. The VSWR results of the proposed antenna are measured using a calibrated Agilent vector network analyzer N5230A. The radiation performance of the antenna is measured in an anechoic chamber.

A. VSWR

Fig. 8 depicts the comparison between the simulated and measured VSWR results, which shows a good agreement. It is observed that the proposed antenna has a very wide bandwidth from 3.56 GHz to 18.5 GHz in simulated results, whereas the measured VSWR is less than 2.5 from 3.78 GHz to 18.54 GHz. The corresponding fractional bandwidths are 135.4% and 132.3%, respectively.

B. RADIATION PERFORMANCE

The simulated and measured 2D radiation patterns of the proposed antenna in the E-plane and H-plane at the frequencies of 4 GHz, 7 GHz, 10 GHz, 12 GHz, 14 GHz and 17 GHz are shown in Fig.9. Generally, the simulated and measured patterns are in good agreement. It is clear that the proposed antenna exhibits good end-fire radiation pattern, and the radiation beam angle in the E-plane tilts away from the end-fire direction to an angle of around 38 degrees at all frequencies owing to the finite ground size. In the H-plane, an approximately symmetrical pattern is observed, which is attributed to the symmetric geometry with respect to the y-axis.

Fig.10 plots the simulated and measured peak realized gain versus frequency for the proposed antenna. The peak gain is obtained by choosing the maximum gain value of radiation pattern in the E-plane. As can be observed, within the operating bandwidth from 3.5 GHz to 18 GHz, the simulated

TABLE 2. Performance comparison between the proposed antenna and other reported end-fire antennas.

Reference	VSWR	Lowest operating frequency (λ_L is referencing wavelength)	Impedance bandwidth	Profile size	Gain (dBi)	Polarization	Platform-Embedded
[1]	< 2	5.24 GHz (λ_L =57.2 mm)	117%	> 0.231λ_L	No presented	Horizontal polarization	No
[3]	< 2.5	6.6 GHz (λ_L =45.45 mm)	93%	0.07λ_L	1.5-14.5	Vertical polarization	No
[4]	< 2.5	1.5 GHz (λ_L =200 mm)	127.7%	0.047λ_L	4.5-10	Vertical polarization	No
[5]	< 2	2.95 GHz (λ_L = 101.7 mm)	109%	0.044λ_L	6.5-14.6	Vertical polarization	No
[7]	< 2	6.1 GHz (λ_L =49.2 mm)	~100%	0.062λ_L	4-12	Vertical polarization	No
This work	< 2.5	3.78 GHz (λ_L =79.4 mm)	132.3%	0.063λ_L	5.5-14.1	Vertical polarization	Yes

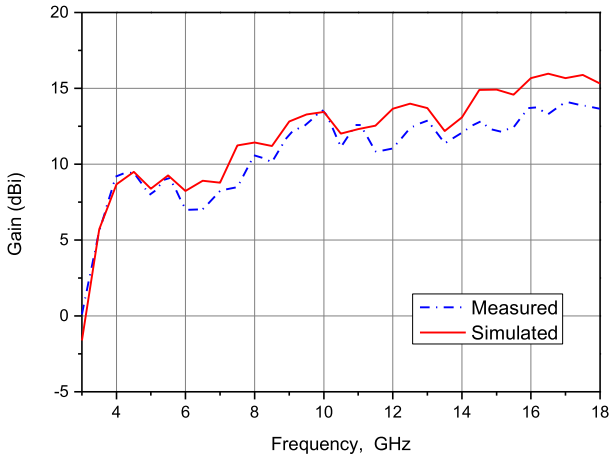

FIGURE 10. Simulated and measured gain results of the proposed surface wave antenna.

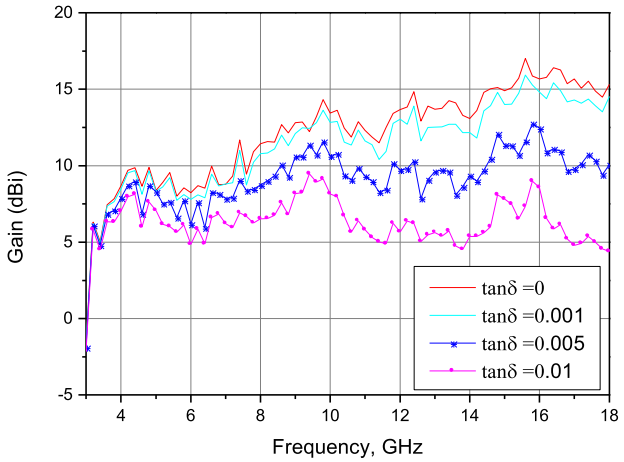

FIGURE 11. Effect of the dielectric loss tangent on the peak realized gain of the proposed surface-wave antenna.

gain varies between 5.73 dBi at 3.5 GHz and 16.2 dBi at 16.5 GHz, while the measured gain varies between 5.5 dBi and 14.1 dBi. Moreover, the simulated and measured gain values are increasing progressively and the measured results are slightly less than the simulated values. Especially within the frequency ranges from 14 GHz to 18 GHz, a large gain discrepancy is noted, which may be attributed to the reason that the measured VSWR from 14 GHz to 18 GHz is much higher than the simulated results so that the total radiated energy is smaller. Other possible factors attributing to the discrepancies between simulated and measured results include the fabrication tolerance, the alignment error of our measurement platform, and the error of material parameters of the ceramic substrate. In particular, the dielectric loss tangent ($\tan\delta$) of our commercial ceramic material has a large effect on the gain, which is illustrated in Fig.11. It is seen clearly that with an increasing loss tangent of the ceramic slab, the gain is decreased (for example, gain from 13.04 dBi for loss tangent of 0.001 to 5.7 dBi for loss tangent of 0.01 at 12 GHz; gain from 14.3 dBi for loss tangent of 0.001 to 4.8 dBi for loss tangent of 0.01 at 17 GHz). Therefore, the discrepancy between simulated and measured results is still within a reasonable range by considering all these factors.

C. PERFORMANCE COMPARISON

The performance of the proposed antenna is compared with previous designs in the literature in terms of fractional bandwidth, profile size, gain, polarization, and conformal requirement, as shown in Table 2. It is seen that our proposed antenna has the widest bandwidth, while maintaining a low profile. More importantly, our designed antenna is embedded into a large aluminum platform, which is then suitable for practical conformal environments. The design in [1] has a large profile, though its bandwidth is more than 117%. The antenna in [3], constructed by using ridged H-plane horn, uses a three-step ridge to enhance the operating bandwidth, while its bandwidth and profile are still smaller and thicker than those of our proposed antenna. The design in [5] has a very impressive low profile, though its bandwidth is slightly smaller than our antenna. Compared with the work in [7], our proposed antenna has the same profile, while exhibiting much wider bandwidth.

V. CONCLUSION

An end-fire surface-wave antenna with wide bandwidth and low-profile characteristics has been described in this paper.

In order to enhance the operating bandwidth of the surface wave antenna, a gradient MS array together with a small BFCH has been employed to suppress TM higher-order modes excited in a grounded slab at higher frequencies. The final antenna has been fabricated and tested. Measured results show that the MS and BFCH can effectively improve the radiation pattern at higher frequencies. Moreover, the surface wave antenna has a very wide bandwidth from 3.78 GHz to 18.54 GHz with VSWR < 2.5, and retains a low profile of only 5 mm ($\sim 0.063\lambda_L$). Good end-fire radiation pattern and high gain have also been experimentally verified.

REFERENCES

[1] P. Wang, G. Wen, H. Zhang, and Y. Sun, "A wideband conformal end-fire antenna array mounted on a large conducting cylinder," *IEEE Trans. Antennas Propag.*, vol. 61, no. 9, pp. 4857–4861, Sep. 2013.

[2] Y. Zhao, Z. Shen, and W. Wu, "Wideband and low-profile H-plane ridged SIW horn antenna mounted on a large conducting plane," *IEEE Trans. Antennas Propag.*, vol. 62, no. 11, pp. 5895–5900, Nov. 2014.

[3] Y. Zhao, Z. Shen, and W. Wu, "Conformal SIW H-plane horn antenna on a conducting cylinder," *IEEE Antennas Wireless Propag. Lett.*, vol. 14, pp. 1271–1274, 2015.

[4] Z. Hu, Z. Shen, W. Wu, and J. Lu, "Low-profile log-periodic monopole array," *IEEE Trans. Antennas Propag.*, vol. 63, no. 12, pp. 5484–5491, Dec. 2015.

[5] S. Zhang and G. F. Pedersen, "Compact wideband and low-profile antenna mountable on large metallic surfaces," *IEEE Trans. Antennas Propag.*, vol. 65, no. 1, pp. 6–16, Jan. 2017.

[6] L. B. Felsen, "Radiation from a tapered surface wave antenna," *Antennas Propag., IRE Trans. on*, vol. 8, no. 6, pp. 577–586, Nov. 1960.

[7] Z. Chen and Z. Shen, "Wideband flush-mounted surface wave antenna of very low profile," *IEEE Trans. Antennas Propag.*, vol. 63, no. 6, pp. 2430–2438, Jun. 2015.

[8] S. Cho and R. King, "Numerical solution of nonuniform surface wave antennas," *IEEE Trans. Antennas Propag.*, vol. AP-24, no. 4, pp. 483–490, Jul. 1976.

[9] F. Butterfield, "Dielectric sheet radiators," *Trans. IRE Prof. Group Antennas Propag.*, vol. 2, no. 4, pp. 152–158, Oct. 1954.

[10] J. Richmond, L. Peters, and R. Hill, "Surface waves on a lossy planar ferrite slab," *IEEE Trans. Antennas Propag.*, vol. AP-35, no. 7, pp. 802–808, Jul. 1987.

[11] S. X. Ta and I. Park, "Compact wideband circularly polarized patch antenna array using metasurface," *IEEE Antennas Wireless Propag. Lett.*, vol. 16, pp. 1932–1936, 2017.

[12] B. Majumder, K. Krishnamoorthy, J. Mukherjee, and K. P. Ray, "Compact broadband directive slot antenna loaded with cavities and single and double layers of metasurfaces," *IEEE Trans. Antennas Propag.*, vol. 64, no. 11, pp. 4595–4606, Nov. 2016.

[13] H. L. Zhu, S. W. Cheung, K. L. Chung, and T. I. Yuk, "Linear-to circular polarization conversion using metasurface," *IEEE Trans. Antennas Propag.*, vol. 61, no. 9, pp. 4615–4623, Sep. 2013.

[14] T. Cai *et al.*, "Ultra-thin polarization beam splitter using 2-D transmissive phase gradient metasurface," *IEEE Trans. Antennas Propag.*, vol. 63, no. 12, pp. 5629–5636, Dec. 2015.

[15] Y. M. Pan, P. F. Hu, X. Y. Zhang, and S. Y. Zheng, "A low-profile high-gain and wideband filtering antenna with metasurface," *IEEE Trans. Antennas Propag.*, vol. 64, no. 5, pp. 2010–2016, May 2016.

[16] A. A. Salih, Z. N. Chen, and K. Mouthaan, "Characteristic mode analysis and metasurface- based suppression of higher order modes of a 2×2 closely spaced phased array," *IEEE Trans. Antennas Propag.*, vol. 65, no. 3, pp. 1141–1150, Mar. 2017.

[17] J. J. Cadusch, T. D. James, A. Djalalian-Assl, T. J. Davis, and A. Roberts, "A chiral plasmonic metasurface circular polarization filter," *IEEE Photon. Technol. Lett.*, vol. 26, no. 23, pp. 2357–2360, Dec. 1, 2014.

[18] B. O. Zhu *et al.*, "Dynamic control of electromagnetic wave propagation with the equivalent principle inspired tunable metasurface," *Sci. Rep.*, vol. 4, May 2014, Art. no. 4971.

[19] A. R. Mallahzadeh and S. Esfandiarpour, "Wideband H-plane horn antenna based on ridge substrate integrated waveguide (RSIW)," *IEEE Antennas Wireless Propag. Lett.*, vol. 11, pp. 85–88, 2012.

[20] R. E. Collin, *Field Theory of Guided Waves*, 2nd ed. New York, NY, USA: Wiley, 1991, pp. 712–713.

[21] X. Wan, L. Zhang, S. L. Jia, J. Y. Yin, and T. J. Cui, "Horn antenna with reconfigurable beam-refraction and polarization based on anisotropic Huygens metasurface," *IEEE Trans. Antennas Propag.*, vol. 65, no. 9, pp. 4427–4434, Sep. 2017.

PING WANG was born in Chongqing, China. He received the M.S degree in theoretical physics from the Chongqing University of China in 2008 and the Ph.D. degree from the University of Electronic Science and Technology of China in 2013. He is currently a Research Fellow with the School of Electrical and Electronic Engineering, Nanyang Technological University, Singapore, and also with the Chongqing University of Posts and Telecommunications, China. His current research interests include patch antennas, wide band antennas, and arrays.

ZHONGXIANG SHEN received the B.Eng. degree from the University of Electronic Science and Technology of China, Chengdu, China, in 1987, the M.S. degree from Southeast University, Nanjing, China, in 1990, and the Ph.D. degree from the University of Waterloo, Waterloo, Ontario, Canada, in 1997, all in electrical engineering.

From 1990 to 1994, he was with the Nanjing University of Aeronautics and Astronautics, China. He was with Com Dev Ltd., Cambridge, Canada, as an Advanced Member of Technical Staff in 1997. He spent six months each in 1998, first with the Gordon McKay Laboratory, Harvard University, Cambridge, MA, and then with the Radiation Laboratory, University of Michigan, Ann Arbor, MI, USA, as a Post-Doctoral Fellow. In 1999, he joined Nanyang Technological University, Singapore, where he is currently a Professor with the School of Electrical and Electronic Engineering. He has authored or co-authored over 140 journal papers (among them 80 were published in IEEE Journals) and presented over 150 conference papers. His research interests include design of small and planar antennas for various wireless communication systems, analysis and design of frequency-selective structures, and hybrid numerical techniques for modeling RF/microwave components and antennas.

Dr. Shen served as the Chair of the IEEE MTT/AP Singapore Chapter in 2009. He was the Chair of the IEEE AP-S Chapter Activities Committee from 2010 to 2014. He is currently the Secretary of the IEEE AP-S and an Associate Editor of the IEEE TRANSACTIONS ON ANTENNAS AND PROPAGATION.